J. Fluid Mech. (1986), *vol.* 170, *pp.* 253–264
Printed in Great Britain

A hybrid method for transonic flow past multi-element aerofoils

By M. G. HILL† AND N. RILEY
School of Mathematics and Physics, University of East Anglia, Norwich NR4 7TJ, UK

(Received 19 October 1985)

A method for calculating transonic potential flow past a multi-element aerofoil configuration is presented. The method is a hybrid method that is based upon a compressible-flow panel method, valid for subcritical flow, and a finite-difference method that is suitable for supercritical flow calculations. The effectiveness of the proposed method is demonstrated, first by application to a single aerofoil and then to a three-element aerofoil.

1. Introduction

In a recent paper, Hill, Riley & Morton (1968) have described a boundary-integral, or panel, method of solution of the two-dimensional potential equation for compressible flow. The method is, in principle, directly analogous to the widely used panel methods for incompressible potential flow (Hess 1973; Hess & Smith 1966), and is based in particular upon a formulation of Newling (1977). Although the method leads to a solution of the potential equation for compressible flow, it is limited, in its application, to flows that are subcritical. Examples are given in which the method is applied to flow past single bodies and, more importantly, to compressible flow past multi-element aerofoil configurations.

In the present paper we address ourselves to the problem of finding conservative full potential solutions for transonic flow past multi-element aerofoil configurations. In order to avoid the difficulties of mesh generation, which are encountered if a finite-difference method of solution is adopted for the whole of the flow field, we use a hybrid method of solution that exploits the panel method of Hill *et al.* (1986), and a finite-difference method due to Holst (1979) for supercritical flow. In outline the hybrid method is employed as follows. Within the region in which supercritical flow is known to occur, the finite-difference method of solution is adopted. Outside that region the compressible-flow panel method is used. At a boundary between the regions in which the different methods are employed the solutions are appropriately matched. Since in practice our main concern is with high-lift configurations, we may expect the region of supercritical flow to be limited to a relatively small region on the slat.

The plan of the paper is as follows. In §2 we introduce the governing equations, and outline in more schematic detail the hybrid method of solution. This is followed in §3 by a more detailed description of each of the compressible flow panel, and finite-difference methods. The hybrid method is then applied, in §4, first to flow past a single aerofoil in both sub- and supercritical flow conditions and then to a three-element aerofoil configuration. For the latter the flow becomes supercritical, with an attendant shock wave, over the slat. We compare our solutions for a single

† Present address: Department of Civil Engineering, University College, Swansea, SA2 8PP, UK.

aerofoil with solutions calculated from the method of Garabedian & Korn (1971), and for the three-element aerofoil with solutions obtained by a finite-element method due to King.

2. Equations and solution scheme

We are concerned in this paper with the steady two-dimensional flow of an inviscid compressible fluid past one, or more particularly two or more, shapes of aerodynamic interest. We assume that the fluid is a perfect gas and that the flow is both irrotational and isentropic.

We take the free-stream speed U_1, density at infinity ρ_1, and a typical dimension l of a body in the flow field as reference velocity, density and length respectively. Then, with $\boldsymbol{v} = (u, v) = \boldsymbol{\nabla}\Phi$, the equation satisfied by the potential Φ is, in a Cartesian coordinate system (x, y),

$$\frac{\partial}{\partial x}\left(\rho\frac{\partial \Phi}{\partial x}\right)+\frac{\partial}{\partial y}\left(\rho\frac{\partial \Phi}{\partial y}\right)=0. \tag{2.1}$$

The Bernoulli equation, which is an energy integral of the governing equations, may be written as

$$\rho = \{1+\tfrac{1}{2}(\gamma-1)\,M_1^2(1-q^2)\}^{1/(\gamma-1)} = B(\Phi), \tag{2.2}$$

where $q^2 = u^2+v^2 = |\boldsymbol{\nabla}\Phi|^2$, $M_1 = U_1/a_1$, γ is the ratio of the specific heats and use has been made of the isentropic relation $a^2 = \rho^{\gamma-1}$, where a is the speed of sound made dimensionless with its value a_1 at infinity. Equations (2.1) and (2.2) are to be solved subject to the boundary conditions

$$\Phi \sim x \quad \text{as } |\boldsymbol{x}|\to\infty, \quad \boldsymbol{\nabla}\Phi\cdot\boldsymbol{n} = 0 \quad \text{on } C, \tag{2.3a, b}$$

where we have assumed that the flow at infinity is parallel to the x-axis, and we have denoted by C an internal boundary whose unit normal is $\boldsymbol{n}$. Kutta conditions are applied at the sharp trailing edges of each of the aerodynamic shapes that bound the flow internally to determine the circulation about each shape, and so render the solution unique.

Since (2.1)–(2.3) are nonlinear, iterative schemes are employed in their solution. Our method of solution is a hybrid method, designed specifically to handle supercritical flow past aerodynamic configurations with two or more elements. It employs two solution methods and involves an iteration between them, in addition to the iterations demanded by the nonlinearity of (2.1)–(2.3). The two solution methods are (i) a compressible-flow panel method (CPM) proposed recently by Hill *et al.* (1986), and (ii) a finite-difference method (FDM) due to Holst (1979) and Flores *et al.* (1984). The CPM is based upon a successful panel method for incompressible flow due to Newling (1977), and has been used by the present authors to study the compressible flow past multi-element aerofoil configurations, but in subcritical flow conditions only (to which it is restricted). The FDM is a fully conservative method and is based upon a non-orthogonal coordinate system. For the type of flow under consideration there are potential benefits to be gained from the use of a non-orthogonal computational mesh, as described in §3.2, although to be sure we have not taken advantage of these. We outline the CPM and FDM in §3; for further details of the methods reference may be made to the papers referenced above. In the remainder of this section we describe the manner in which we implement our hybrid scheme.

As we have already made clear, the CPM is only appropriate when the flow conditions are subcritical, and of itself cannot handle supercritical flows. It can be

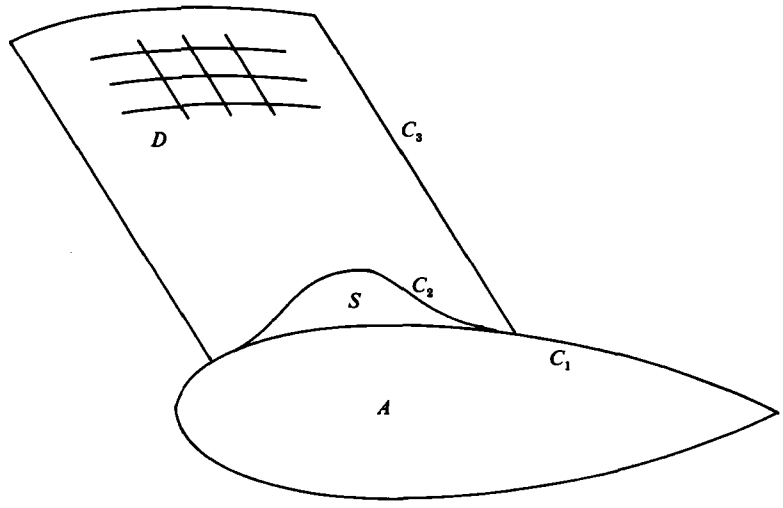

FIGURE 1. A schematic representation of the computational domains.

used, therefore, only for those parts of the flow field in which the flow remains subsonic. Consider figure 1. Here we show an aerofoil shape A whose bounding curve is denoted by C_1, at which the boundary condition (2.3b) is to be applied. The curve C_2, together with part of C_1, bounds a region S in which supercritical flow occurs. The choice of the contour C_2 is not unique, but certain requirements must be satisfied by it. The most obvious of these is that it does indeed include the whole of the region of supersonic flow, and this is most easily tested by monitoring the local Mach number on C_2. The other requirement that is important for the succesful application of the panel method is that where C_2 and C_1 meet, their slopes also coincide. Failure to meet this requirement resulted in numerical oscillations at the junction of C_2 and C_1. For the examples that we discuss in §4, the dimensions of the region S are up to almost 50% chord in length and of the order of the maximum aerofoil thickness in height. In principle the CPM can be applied to the flow exterior to the region $A+S$ provided that values of $\partial\Phi/\partial n$ are known on C_2. Next consider the region $D+S$ which is bounded by the curve C_3, together with part of C_1. Within this region, which includes the supercritical part of the flow, the FDM may be used provided that boundary conditions for (2.1) are available along C_3. The missing boundary conditions for each method are provided by the solution from the other method in an iterative manner as follows. As a first approximation we assume that the flow is the undisturbed free stream. From this we are able to calculate values of $\partial\Phi/\partial n$ on C_2. Using these values, together with (2.3), we then calculate the flow exterior to the region $A+S$ using the CPM. From that solution the potential is not given directly, but can be calculated from the velocities to give Φ along C_3. With $\partial\Phi/\partial n = 0$ on C_1 the FDM may then be used to determine the solution for this mixed boundary-value problem within the region $D+S$, and from that solution we are able to estimate new values of $\partial\Phi/\partial n$ on C_2 for use with the CPM, and so on. At each stage a check is made to ensure that subcritical flow conditions are maintained on C_2.

The method by which each of the CPM and FDM is implemented is outlined in §3; further details of these methods may be found in Hill *et al.* (1986) and Flores *et al.* (1984) respectively. Results obtained by our hybrid method are discussed in §4.

For a single aerofoil it is not necessary to use other than the FDM, since a suitable computational grid may be established by, for example, mapping the flow field to

the inside of a circle to whose boundary the curve C_1 transforms. Similarly, for a two-element configuration Suddhoo (1985) has shown that the flow field may be transformed to the annulus between two concentric circles, each boundary of which represents the boundary of one of the elements. As for the case of a single element, a polar grid is conveniently used for the computations. To generate a satisfactory computation grid for more than two elements in any configuration is a task that has not yet been satisfactorily carried out, and it is in such situations that the advantages of the present method become apparent. Alternative methods of solution to that proposed here for multi-element configurations are the finite-element method of D. A. King (1985 private communication, British Aerospace, Hatfield), with whose results we are able to make a comparison, and a field panel method due to Oskam (1985). In the latter, (2.1) is written in the form of Poisson's equation and a boundary-integral approach is adopted that yields an expression for Φ that includes a double integral of the source term. Using a finite-volume technique, the relationship between Φ and the source term is also established, from the governing equation, at field points in a region in which compressibility effects are most significant and beyond which the flow is assumed to be incompressible. If the double integral is also approximated numerically at the field points the source term may be evaluated and the solution completed using a panel method.

3. Numerical methods

In this section we outline both the compressible panel method of Hill *et al.* (1986) and the finite-difference method of Flores *et al.* (1984).

3.1. *The compressible-flow panel method*

The CPM is based upon the highly successful panel method for incompressible flow of Newling (1977). For incompressible flow the fundamental solutions of (2.1) correspond to the potentials of a line source and a line vortex respectively, and the solution for Φ is constructed as arising from distributions of such singularities over the bounding surfaces C. If the source and vortex strengths are denoted by $\sigma(\boldsymbol{q})$ and $\gamma(\boldsymbol{q})$ respectively, where $\boldsymbol{q}$ is a point on the boundary, then, following an assumption about their symmetry, σ and γ are determined by applying the condition for $\partial\Phi/\partial n$ at the bounding surface.

If we assume that the density is a known function in (2.1), then the analogue of Newling's method for that equation leads to

$$\rho(\boldsymbol{p})\frac{\partial\Phi(\boldsymbol{p})}{\partial x}=\frac{\partial\Phi_\infty(\boldsymbol{p})}{\partial x}+\rho(\boldsymbol{p})\int_C\sigma(\boldsymbol{q})\frac{\partial\Psi}{\partial x}(\boldsymbol{p}-\boldsymbol{q})\,\mathrm{d}q+\rho(\boldsymbol{p})\int_C\gamma(\boldsymbol{q})\frac{\partial\Theta}{\partial x}(\boldsymbol{p}-\boldsymbol{q})\,\mathrm{d}q, \quad (3.1)$$

for the x-component of velocity, with a similar expression for the y-component, where $\boldsymbol{p}$ is a point in the flow field, so that $\boldsymbol{p}\neq\boldsymbol{q}$, and $\Phi_\infty = x$. If $\boldsymbol{p}$ lies on C then for the normal derivative of Φ on C we have

$$\rho(\boldsymbol{p})\frac{\partial\Phi(\boldsymbol{p})}{\partial n_p}=\frac{\partial\Phi_\infty(\boldsymbol{p})}{\partial n_p}+\pi\rho(\boldsymbol{p})^{\frac{1}{2}}\sigma(\boldsymbol{p})+\rho(\boldsymbol{p})\int_C\sigma(\boldsymbol{q})\frac{\partial\Psi}{\partial n_p}(\boldsymbol{p}-\boldsymbol{q})\,\mathrm{d}q$$
$$+\rho(\boldsymbol{p})\int_C\gamma(\boldsymbol{q})\frac{\partial\Theta}{\partial n_p}(\boldsymbol{p}-\boldsymbol{q})\,\mathrm{d}q. \quad (3.2)$$

In (3.1) and (3.2), Ψ and Θ are the fundamental solutions of (2.1) for a given density distribution $\rho(x,y)$, and are the analogues of the source and vortex solutions for incompressible flow. They are related to a complex function F as

$$F=\rho^{\frac{1}{2}}(\Psi+\mathrm{i}\Theta), \quad (3.3)$$

which itself may be written as

$$F(z,w;\delta,\bar{\delta}) = \log(z-\delta) + G(z,w;\delta,\bar{\delta}), \tag{3.4}$$

where $z = x+\mathrm{i}y$, $w = x-\mathrm{i}y$, with (x,y) now representing the analytic continuation of the real variables into the complex plane, and $(\delta,\bar{\delta})$ representing the point $\boldsymbol{p}$ in (3.2). G satisfies the Volterra integral equation

$$G(z,w;\delta,\bar{\delta}) = \int_{\delta}^{z}\int_{\bar{\delta}}^{w} \hat{\rho}^{-\frac{1}{2}} \frac{\partial^2 \hat{\rho}^{\frac{1}{2}}}{\partial t\,\partial \tau} \log(t-\delta)\,\mathrm{d}\tau\,\mathrm{d}t + \int_{\delta}^{z}\int_{\bar{\delta}}^{w} \hat{\rho}^{-\frac{1}{2}} \frac{\partial^2 \hat{\rho}^{\frac{1}{2}}}{\partial t\,\partial \tau} G(t,\tau;\delta,\bar{\delta})\,\mathrm{d}\tau\,\mathrm{d}t, \tag{3.5}$$

where a caret denotes the analytic continuation. The derivation and solution of the integral equation (3.5), and hence the determination of Ψ and Θ, is discussed in detail by Hill *et al.* (1986), and in a more general context by Hill & Porter (1985). Before we discuss the solution of the Fredholm integral equation (3.2) for the distributions σ and γ, we note that (3.1) and (3.2) are appropriate to a given density distribution ρ. Of course, ρ is not determined *a priori*, and the variables Φ, ρ must satisfy both (2.1) and (2.2) simultaneously. To achieve this we proceed iteratively as follows. Initially we set $\rho \equiv 1$ and determine σ and γ from (3.2) in the manner to be described below. The velocity components $\partial\Phi/\partial x$, $\partial\Phi/\partial y$ are then determined as in (3.1), which enables us to obtain a new estimate of ρ from (2.2), from which updated values of Ψ and Θ may be obtained from (3.3)–(3.5). New values of σ and γ may then be obtained from (3.2), and so on. In the solutions given by Hill *et al.*, for subcritical flow past multi-element configurations, seven such iterative cycles achieved convergence. It remains to indicate how (3.2) is solved for the distributions σ and γ.

The boundary of the domain, C, which may consist of one or more elements and which does not necessarily coincide everywhere with a physical boundary, as for example C_2 in figure 1, is discretized so that it is represented by a sequence of boundary elements or 'panels'. We choose these panels as straight-line segments, and, with reference to an aerodynamic shape, we represent each of the upper and lower surfaces by N such panels, making $2N$ panels in all. We identify corresponding panels on the upper and lower surfaces by dividing the straight line joining the nose and the trailing edge into N, not necessarily equal, segments and take as our panels the linear projections of these onto C. The source strength is taken as piecewise constant with $\sigma = \sigma_i$ on the ith panel, and the vorticity distribution is taken to be a continuous piecewise linear function. We denote by γ_{i-1} and γ_i the vortex strengths at each end of the ith panel, and if a sharp trailing edge corresponds to $i = 0$ we set $\gamma_0 = 0$ to satisfy the Kutta condition. The integrals in (3.2) are now evaluated numerically over all the panels into which C has been divided. The left-hand side of (3.2) is evaluated from (2.3*b*) on C_1, and the solution obtained from the FDM on C_2. There result $2N$ equations that are linear in the $4N$ unknown quantities σ_i and γ_i. To make the system determinate, the source and vortex densities on opposite panels on the upper and lower surfaces are prescribed to be equal. The $2N$ unknown quantities may then be determined by standard methods from the $2N$ equations. The iterations that yield Φ and ρ from the CPM are not continued to the point at which convergence is achieved at each stage of the overall iterative cycle. In practice, about seven iterations have been completed before attention has been turned to the region $D+S$, in which the solution is obtained by the FDM that we now describe.

3.2. *The finite-difference method*

The finite-difference method that we have adopted is due to Holst (1979) and Flores *et al.* (1984); a key feature of this method is the use of a non-orthogonal coordinate

system (ξ, η). Here (see figure 1) we choose the aerofoil surface as the line $\eta = 0$ with lines parallel to this as $\eta =$ constant. Parallel straight lines intersecting $\eta = 0$ are taken as the lines $\xi =$ constant. The angle that these make with some fixed direction may be varied, which may be advantageous in some situations. For example in a multi-element configuration, if supercritical flow occurs at the leading edge of the main aerofoil then it is important to ensure that the trailing edge of the slat does not intrude into the computational domain $D+S$. This can be achieved by suitably aligning the straight lines $\xi =$ constant. (In fact none of the examples that we present in §4 exhibit this feature.) If $(\tilde{x}, \tilde{y})$ denote some arbitrary rectangular coordinates with the aerofoil surface given by $\tilde{y} = f(\tilde{x})$ then we take

$$\xi = (\tilde{x}-\tilde{x}_0)/L, \quad \eta = \{\tilde{y}-f(\tilde{x})\}/L. \tag{3.6}$$

In terms of these new coordinates we may write (2.1) as

$$\frac{\partial}{\partial \xi}\left(\frac{\rho U}{J}\right)+\frac{\partial}{\partial \eta}\left(\frac{\rho V}{J}\right) = 0, \tag{3.7}$$

where

$$\left.\begin{aligned} U &= A_1 \Phi_\xi + A_2 \Phi_\eta, \quad & V &= A_2 \Phi_\xi + A_3 \Phi_\eta, \\ A_1 &= \xi_{\tilde{x}}^2 + \xi_{\tilde{y}}^2, & A_2 &= \xi_{\tilde{x}}\eta_{\tilde{x}} + \xi_{\tilde{y}}\eta_{\tilde{y}}, \\ A_3 &= \eta_{\tilde{x}}^2 + \eta_{\tilde{y}}^2, & J &= \xi_{\tilde{x}}\eta_{\tilde{y}} - \xi_{\tilde{y}}\eta_{\tilde{x}}, \end{aligned}\right\} \tag{3.8}$$

and a subscript variable denotes differentiation with respect to that variable. For the finite-difference method of Holst (1979), which we outline now, we use a subscript notation such that (i,j) denotes the point whose coordinates are $(i\delta\xi, j\delta\eta)$, and we take $\delta\xi = \delta\eta$. Holst approximates (3.7) as

$$\delta_\xi\left(\frac{\tilde{\rho} U}{J}\right)_{i+\frac{1}{2},j} + \delta_\eta\left(\frac{\rho V}{J}\right)_{i,j+\frac{1}{2}} = 0, \tag{3.9}$$

where the operators

$$\left.\begin{aligned} \delta_\xi(\ )_{i+\frac{1}{2},j} &= (\ )_{i+\frac{1}{2},j} - (\ )_{i-\frac{1}{2},j}, \\ \delta_\eta(\ )_{i,j+\frac{1}{2}} &= (\ )_{i,j+\frac{1}{2}} - (\ )_{i,j-\frac{1}{2}}, \end{aligned}\right\} \tag{3.10}$$

are second-order, and

$$\tilde{\rho}_{i+\frac{1}{2},j} = (1-\nu_{i+k,j})\rho_{i+\frac{1}{2},j} + \nu_{i+k,j}\rho_{i+2k-\frac{1}{2},j}, \tag{3.11}$$

with

$$k = \begin{cases} 0 & (U_{i+\frac{1}{2},j} \geqslant 0), \\ 1 & (U_{i+\frac{1}{2},j} < 0), \end{cases}$$

$$\nu_{i,j} = \max\left\{0, 1-\left(\frac{M_c}{M}\right)^2\right\}_{i,j}, \tag{3.12}$$

where M is the local Mach number and M_c is a constant. Following Jameson (1979), we take $M_c = 0.9$ in our calculations. The boundary condition (2.3*b*) now becomes

$$\Phi_\xi = -\frac{A_3}{A_2}\Phi_\eta \quad \text{at } \eta = 0. \tag{3.13}$$

For a given density distribution the finite-difference equations derived from (3.9) (using (3.8)) and (3.13), using second-order accurate differences, together with (2.3*a*) applied at a large but finite distance, are solved using a standard SOR method. The solution may then be used in (2.2) to update the density, and such an iterative

procedure continued until a satisfactorily converged solution is realized. (For further details of the method see Holst (1979) and Flores *et al.* (1984).)

Our method is based firmly upon that of Holst outlined above, with the following three differences. First, we have used fourth-order-accurate difference schemes throughout, rather than those of second order adopted by Holst in order to improve the accuracy of the solution. Secondly, our computational domain, $D+S$ in figure 1, is much smaller than Holst's, so that the freestream condition cannot be applied at the outer boundary. Thus, in addition to the boundary condition (2.3*b*) on C_1, we require a condition on C_3. This we have chosen to be the value of Φ calculated from the CPM; it is derived by integrating the component of velocity parallel to the appropriate coordinate line along the length of C_3. Thirdly, we have taken $M_c \neq 1$ (Jameson 1979) in (3.12), whereas Holst chooses $M_c = 1$. Like Holst, then, we have a mixed boundary-value problem, but in a simply connected domain that, with an equal number of grid points in each of the coordinate directions, is a square in (ξ, η)-space. The relationship between C_2 and C_3 (see figure 1) in our procedure is such that C_2 intersects C_1 between 2 and 5 grid points in from C_3 at each end.

4. Examples

In this section we present examples that are calculated using the techniques that we have described above.

Although our hybrid technique has been developed to calculate the flow past multi-element configurations, we consider first the flow past a single aerofoil, namely the NACA 0012. Solutions using the method of Garabedian & Korn (1971, hereinafter referred to as GK) have kindly been made available to the present authors by R. C. Lock. The computational domain for these calculations is the interior of a circle to which the flow field is mapped. The discretization leads to 160 equally spaced grid points on the circle, which corresponds to the aerofoil, and the transformation gives a higher density of points at the leading and trailing edges of the aerofoil than elsewhere. For the CPM we have taken 160 panels whose endpoints coincide on C_1 with the gridpoints of the GK calculation. The panels on C_2 are such that when projected onto C_1 they coincide with the panels we have defined there.

The first case we consider is a case for which flow conditions are almost critical, and for which a solution using the CPM alone has already been presented by Hill *et al.* (1986). Within the domain $D+S$ of figure 1 we have worked with two grid sizes and have achieved this in the following manner. The coarse grid has 80×80 grid points extending along 50 % of the aerofoil chord from the leading edge, with the 'bubble' S extending along 20 % of the chord from a point two mesh lengths away from the leading edge, and with a thickness equal to that of the maximum thickness of the aerofoil. The fine mesh also has 80×80 grid points, but now this extends along only 20 % of the chord from the leading edge, with the bubble S, now of thickness half that of the maximum aerofoil thickness, extending along 10 %. In the iterative cycles, using the two methods, we have employed 7 iterations each time the CPM is used, while for the FDM we have after each 10 iterations monitored the maximum difference between the solutions and terminated these iterations when that difference is less than 5 % of the computed quantity. To achieve the graphical accuracy of figure 2 required five overall iterative cycles. This figure compares the solution obtained in the manner described above with the GK solution over 10 % of the chord, and it is apparent that closer agreement is achieved with the finer mesh. The overall lift coefficient differs from that of the GK solution by 3.5 % for the coarse-mesh solution,

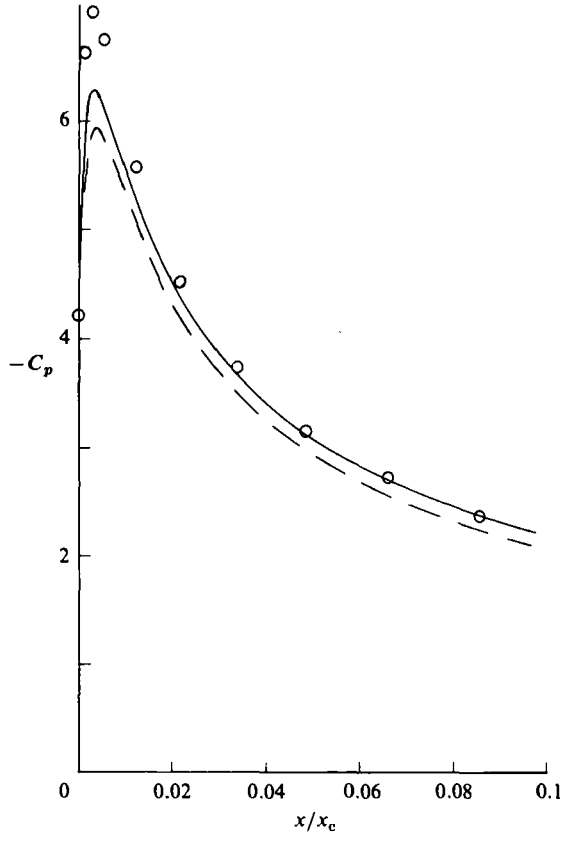

FIGURE 2. The pressure distribution over the upper surface, and close to the leading edge, of the NACA 0012 aerofoil section for $M_1 = 0.3$, and incidence $\alpha = 10°$: ———, coarse-mesh solution; ——, fine-mesh solution; ○, Garabedian & Korn (1971) solution. The chord length is denoted by x_c in all our examples.

and 2.6% for the fine mesh. It is also worth recording that the fine-mesh solution is indistinguishable from that using the CPM alone, with 160 panels, as reported by Hill *et al.* (1986).

The second example for which we present results is also based on the NACA 0012 aerofoil section, but now in supercritical flow conditions. The computational domain $D+S$ of figure 1 and the bubble S are chosen as for the fine-mesh solution described above, except that, while we have continued to use 160 panels, we have used three grid sizes, namely 40×40, 60×60 and 80×80, within $D+S$. The iterative method of solution that was described for the subcritical-flow example was again employed, but now the overall iterative cycles were extended until accuracy to four significant figures was achieved. This required some fifteen overall iterative cycles. We have again made a comparison with a solution obtained by the method of Garabedian & Korn (1971), and for the 80×80 grid we record a difference of 3.9% in the lift coefficient between the two solutions. Figure 3 shows detail of the pressure distribution in the neighbourhood of the shock wave, where we have included the results from all three of our computational meshes together with the solution from the GK method. We see that our solutions predict a shock position and strength that are in broad agreement with the GK solution, but that, as the mesh size decreases, our calculations yield a better resolution of the shock wave, as we might expect.

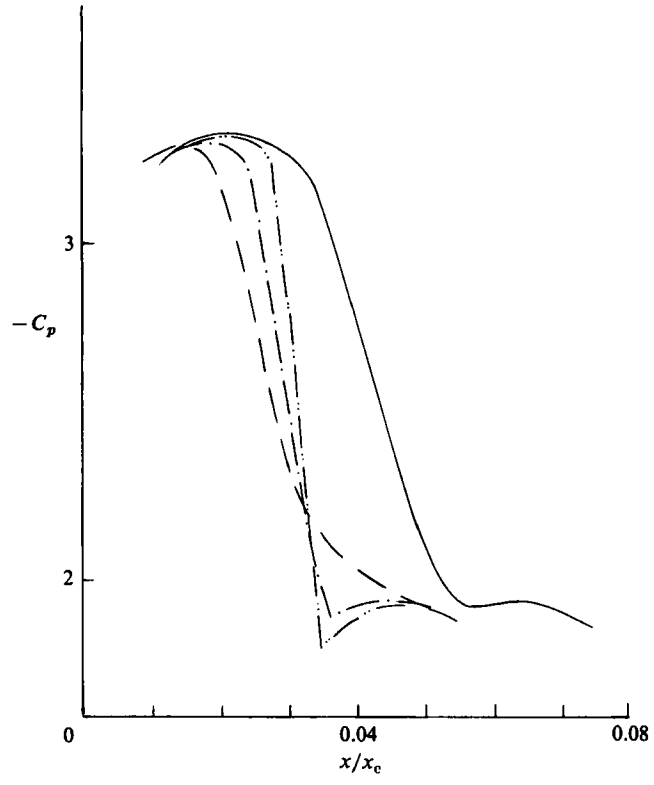

FIGURE 3. The shock wave on the NACA 0012 aerofoil section for $M_1 = 0.5$, $\alpha = 6°$. ——, Garabedian & Korn (1971); – – –, present method with 40×40 mesh; —·—, 60×60; —··—, 80×80.

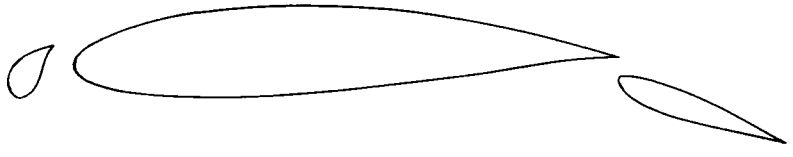

FIGURE 4. The Suddhoo (1985) three-element aerofoil.

The above calculations for a single aerofoil were carried out to demonstrate that the hybrid method described in §§3 and 4 can yield accurate solutions in high subsonic, and transonic, flow conditions. Just as in the subcritical-flow calculations of Hill *et al.* (1986), there is no difficulty in extending the method to multi-element configurations, apart from the obvious increase in computational time that is required as the number of elements increases.

As an example of the method applied to a multi-element configuration we consider the flow past the three-element configuration shown in figure 4. This configuration has been devised by Suddhoo (1985) from a conformal transformation of three circles, and an exact solution is given by him for incompressible flow. We present solutions here, in figures 5 and 6, for two freestream Mach numbers, namely $M_1 = 0.22$ and 0.2 respectively. For the latter case, supercritical flow conditions are just achieved on the slat, while for the higher Mach number a fairly strong shock wave forms on the slat, as is clearly seen in figure 5(*a*). In these calculations we have deployed 60

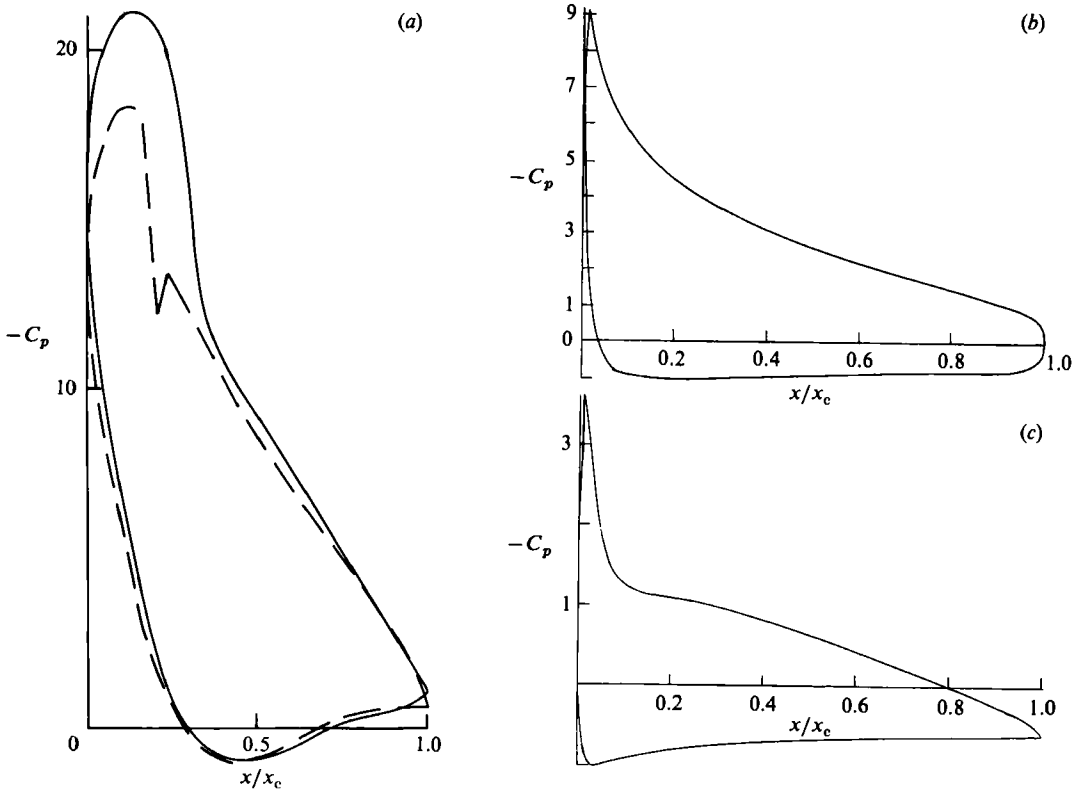

FIGURE 5. Pressure distribution over the three-element aerofoil for $M_1 = 0.22$, $\alpha = 20°$. (*a*) The slat: ——, King (1985, private communication); – – – –, present method with 80 panels on the slat. (*b*) The main aerofoil. (*c*) The flap.

panels on the main aerofoil and flap, with 80 on the slat. The computational domain $D+S$ now extends over 65% of the slat, with S extending over 45% of it and of thickness equal to that of the maximum slat thickness. An 80×80 computational mesh is used within $D+S$. The method of implementation of the CPM and FDM is as described above for the case of a single aerofoil. To achieve the accuracy represented by figures 5 and 6, twenty overall iterative cycles were employed. For this example we have been able to make a comparison with results kindly made available to us by D. A. King using a finite-element method that is currently under development. For the particular example under consideration, 8190 computational nodes have been used with 64 on the slat, 122 on the main aerofoil and 74 on the flap. On the main aerofoil and flap the results obtained by the finite-element method are indistinguishable, except for small differences close to the suction peak, from those shown in figures 5(*b*, *c*) derived from the present method. On the slat, however (see figure 5(*a*)), there are significant differences. Both methods predict the same shock-wave location, defined as the suction peak. However, the finite-element method gives a less clearly defined shock wave than the present method, which suggests that our computational mesh in $D+S$ is sufficiently fine, while the mesh for the finite-element method is not fine enough, to resolve the shock adequately. The difference in suction peak may have several sources. We first note that the difference persists throughout the Mach-number range, where for subcritical flow our results are derived by the CPM alone (Hill *et al.* 1986). In the limiting case of incompressible

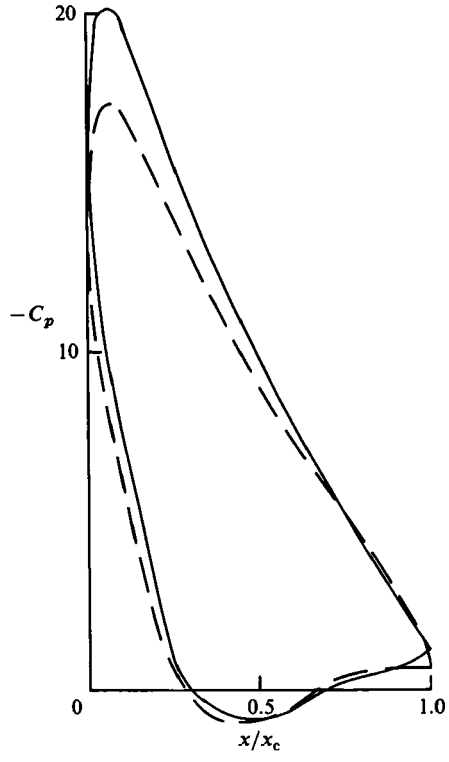

FIGURE 6. Pressure distribution over the slat of the three-element aerofoil for $M_1 = 0.2$, $\alpha = 20°$: ——, King (1985); – – –, present method with 80 panels.

flow the peak suction is slightly overestimated by the finite-element method and underestimated by the panel method, when compared with the exact result due to Suddhoo (1985). It has been demonstrated by Hill *et al.* (1986) that for the CPM, sufficiently fine panelling is required if high suction peaks are to be accurately resolved, and this is known to be a feature of the method as originally devised in its incompressible form. For example, with the NACA 0012 aerofoil at incidence $\alpha = 10°$, and critical Mach number, the peak suction falls short of that predicted by the method of Garabedian & Korn (1971) by 21.5% when 80 panels are used and by only 8.5% when 160 panels are used. For the case under consideration the peak suction is less than that predicted by the finite-element method by 14%. For the lower freestream Mach number, $M_1 = 0.2$, the same differences in pressure distribution are in evidence in figure 6.

All the results presented above have been obtained on a VAX 11/780 computer at the University of East Anglia.

5. Conclusions

In this paper we have devised a hybrid method of solution for transonic flow past multi-element aerofoil configurations. The method of solution is based upon a compressible-flow panel method for subcritical regions of flow, and a finite-difference method for those parts of the flow field that become supercritical. The solutions from the different flow regimes are matched at a common boundary between them. The solutions that are obtained in this way are exact in the sense that no approximations,

other than numerical approximations, are made to the governing equations (2.1) and (2.2). The method is applied to a single-element aerofoil, and to a three-element aerofoil, and comparisons that are made with other available solutions demonstrate the effectiveness of the method. There is, in principle, no limitation upon the number of elements that may be included in a configuration.

Financial support for this project from SERC, within the framework of the BAe/RAE high-lift wing initiative, is gratefully acknowledged, as are helpful discussions with R. C. Lock, J. H. B. Smith, B. R. Williams of RAE and D. A. King of BAe (Hatfield).

REFERENCES

FLORES, J., HOLST, T. L., KWAK, D. & BATISTE, D. M. 1984 *AIAA J.* **22**, 1027.

GARABEDIAN, P. R. & KORN, D. G. 1971 *Commun. Pure Appl. Maths* **24**, 841.

HESS, J. L. 1973 *Comp. Meth. Appl. Mech. Engng* **2**, 1.

HESS, J. L. & SMITH, A. M. O. 1966 *Prog. Aero. Sci.* **8**, 1.

HILL, M. G. & PORTER, D. 1986 The numerical determination of fundamental solutions of elliptic equations. *IMA J. Numer. Anal.* (to be published).

HILL, M. G., RILEY, N. & MORTON, K. W. 1986 *J. Fluid Mech.* **165**, 231.

HOLST, T. L. 1979 *AIAA J.* **17**, 1038.

JAMESON, A. 1979 In *Proc. AIAA Computational Fluid Dynamics Conf., Williamsburg*, p. 122.

NEWLING, J. C. 1977 *Hawker Siddeley Aviation Report*, HSA-MAE-R-FDM-0007.

OSKAM, B. 1985 *AIAA J.* **23**, 1327.

SUDDHOO, A. 1985 Inviscid compressible flow past multi-element aerofoils. Ph.D. thesis, Manchester University.